A force-based protein biochip

K. Blank*, T. Mai*, I. Gilbert*, S. Schiffmann*, J. Rankl*, R. Zivin†, C. Tackney‡, T. Nicolaus*, K. Spinnler*, F. Oesterhelt*, M. Benoit§, H. Clausen-Schaumann*, and H. E. Gaub§¶

*nanotype, Lochhamer Schlag 12, 82166 Gräfelfing, Germany; †Drug Discovery, Johnson & Johnson Pharmaceutical Research & Development, Raritan, NJ 08869; ‡Ortho-Clinical Diagnostics, Raritan, NJ 08869; and §Lehrstuhl für Angewandte Physik and Center for NanoScience, Amalienstrasse 54, 80799 Munich, Germany

Communicated by Heinrich Rohrer, IBM Zurich Research Laboratory, Wollerau, Switzerland, August 4, 2003 (received for review June 1, 2003)

A parallel assay for the quantification of single-molecule binding forces was developed based on differential unbinding force measurements where ligand–receptor interactions are compared with the unzipping forces of DNA hybrids. Using the DNA zippers as molecular force sensors, the efficient discrimination between specific and nonspecific interactions was demonstrated for small molecules binding to specific receptors, as well as for protein–protein interactions on protein arrays. Finally, an antibody sandwich assay with different capture antibodies on one chip surface and with the detection antibodies linked to a congruent surface via the DNA zippers was used to capture and quantify a recombinant hepatitis C antigen from solution. In this case, the DNA zippers enable not only discrimination between specific and nonspecific binding, but also allow for the local application of detection antibodies, thereby eliminating false-positive results caused by cross-reactive antibodies and nonspecific binding.

Previous studies have shown that unbinding forces between molecular interaction partners provide novel and extremely valuable information on the nature of this interaction: specific versus nonspecific interactions and differences in binding modes can be resolved, and even energetically equivalent interactions can be discriminated by forced unbinding (1–5). Moreover, because the binding partners are forced apart, the kinetics of the experiment can be chosen according to assay requirements, and even strong binders, where the spontaneous off-reaction takes weeks or more, may be separated in fractions of seconds (6, 7). Nevertheless, the widespread use of force-based discrimination in bioanalytical applications has been hindered by the limited throughput of these techniques and the high experimental burden imposed by complicated and expensive instrumentation like atomic force microscopes (AFM), optical traps, or the like (8–12). Highly parallel micrometer and submicrometer cantilever arrays, which are currently being developed, might increase the throughput of AFM-based force spectroscopy in the future (13–15). In this study, however, we used a format that not only measures unbinding forces on the single-molecule level in a parallel format, but that is also compatible with standard chip based assays. Here we briefly describe the assay. A more detailed description of the assay is given elsewhere (16).

In standard single-molecule force spectroscopy assays, one of the binding partners is linked to an actuator and the other to a force sensor. The molecules are brought into contact to allow for binding, and on separation the force is recorded as a function of the separation of actuator and force sensor until the bond ruptures (17). In all technical realizations of this principle, the force resolution is limited by thermal fluctuations, which couple into the system via the force sensors (18, 19). We have shown in the past that miniaturization of the force sensors increases their sensitivity (20). Consequently, we employ a single molecule as force sensor in the new format, which is described here. To further improve the force resolution, we implemented a differential measurement format, where the unbinding force of the measured molecular bond is directly compared with the unbinding force of a known reference bond. Both improvements are merged in our Congruent Force Intermolecular Test (C-FIT) format: a molecular chain consisting of the sample bond, a known reference bond, which serves as force sensor, and a reporter molecule, e.g., a fluorescence label, is formed. The ends of this chain are covalently grafted to two surfaces via polymer spacers. During separation of the two surfaces, the force along the chain increases and the bonds are increasingly loaded with the same force until the weaker of the two bonds ruptures. As a result, after separation of the surfaces the reporter molecule is found at the side of the ruptured chain, containing the stronger bond. Thermal fluctuations broaden this yes/no discrimination by force differences on the order of k_BT/l, where l is the characteristic width of the binding potential: the separation between potential minimum and barrier (21).

Obviously, such experiments are primed to be carried out in parallel by using a chip format, with identical molecular chains within each spot and different types of molecules in different spots of the chip. Counting the reporters on either surface, e.g., by counting fluorophores or alternatively measuring fluorescence intensities, then provides a measure for the relative unbinding forces. Analogous to previous studies, bond rupture probabilities may then be calculated taking into account molecular details like spacer lengths and separation rates to correlate the measured unbinding ratios to thermodynamically defined properties such as equilibrium constants and off-rates (7, 21–23).

Methods

Immobilization of Proteins on Slides (Bottom Surface). Proteins and antibodies were purchased from Roche Diagnostics, Biotrend (Cologne, Germany), Calbiochem, Pierce, Biomol (Hamburg, Germany), and pab productions (Hebertshausen, Germany). Hepatitis C virus (HCV) antibodies and the corresponding antigen were provided by Johnson & Johnson. CSS Aldehyde slides (Genetix, Hampshire, U.K.) were incubated with 6 mM $HCl{\cdot}NH_2$-PEG-COOH (3,400 g/mol; Shearwater Polymers, Huntsville, AL; PEG, polyethylene glycol). The resulting Schiff bases were then reduced by using 1% aqueous $NaBH_4$ (VWR Scientific). Alternatively, epoxy slides (Quantifoil Micro Tools, Jena, Germany) were treated with pure diamino PEG (2,000 g/mol; Rapp Polymere, Tübingen, Germany) by melting the diamino PEG and incubating it onto the surface at 75°C for 24 h. The remaining amino groups were then converted into carboxy groups by incubating the slides in a solution of 5 M glutaric anhydride in dry DMF overnight (24). For both types of slides the carboxy groups of the PEG were then activated with a solution containing 50 mM 1-ethyl-3-(3-dimethylaminopropyl)-carbodiimide hydrochloride (EDC; Sigma) and 50 mM *N*-hydroxysuccinimide (NHS; Sigma). The proteins were spotted immediately onto the activated surface. Antibodies were spotted in a concentration of 200 μg/ml. The antigens were spotted in concentrations between 20 and 100 μg/ml. After 1 h of incubation, the slides were washed with PBS (Roche Diagnostics)

Abbreviations: HCV, hepatitis C virus; PDMS, poly(dimethylsiloxane); PEG, polyethylene glycol.

¶To whom correspondence should be addressed. E-mail: hermann.gaub@physik.uni-muenchen.de.

www.pnas.org/cgi/doi/10.1073/pnas.1934928100

containing 0.05% Tween 20 (VWR Scientific). Free reactive groups were blocked in PBS containing 2% BSA (Roth, Karlsruhe, Germany) overnight.

For the sandwich assay the HCV antigen (Johnson & Johnson) was diluted to a concentration of 500 ng/ml in PBS containing 0.4% BSA. This solution was incubated on the slide for 1 h before washing in PBS-Tween 20 (PBST) and PBS.

Immobilization of the DNA Force Sensor Complex on Poly(dimethylsiloxane) (PDMS) (Top Surface). Microstructured PDMS (Sylgard 184, Dow Corning) surfaces were fabricated by using structured 5′ silicon wafers as templates, according to standard procedures (25). The PDMS structures consisted of 100 × 100-μm pads separated by 25-μm-wide and 1-μm-deep grooves to allow for drainage of liquid during the contact process. After cross-linking, the PDMS was cut into 1 × 1-cm pieces (thickness 1 mm) and activated by water plasma treatment. The PDMS was then derivatized with 3-aminopropyldimethylethoxysilane (ABCR, Karlsruhe, Germany) to generate free amino groups and coated with aqueous 18 mM NHS-PEG-COOH (5,000 g/mol; Shearwater Polymers) or 18 mM NHS-PEG-NHS (3,000 g/mol; Rapp Polymere). To bind the amino-labeled receptor oligonucleotide (5′-NH_2-AAA AAA AAA ATC TCC GGC TTT ACG GCG TAT-3′; MWG Biotech, Ebersberg, Germany) to the carboxy-modified surface, 50 mM EDC was added to the solution of the receptor oligonucleotide (25 μM) before it was spotted onto the PEG surface. Subsequently, the samples were rinsed with 1× SSC (Sigma) containing 0.5% SDS (Sigma) and incubated with an aqueous solution of 2% BSA, to reduce nonspecific binding. Cy3-labeled unzip oligonucleotides (5′-Cy3-ATA CGC CGT AAA GCC GGA GAC AGA TAA GAC GCT ACA TGA AAA AAA AAA AA-(haptene)-3′; metabion, Martinsried, Germany) were diluted to 2 μM in 5× SSC and then hybridized for 60 min under a cover slide at room temperature. For all experiments, where antibodies were connected to the DNA force sensor, streptavidin was used to connect biotinylated antibodies to a biotin label at the 3′ end of the unzip oligonucleotide. After incubating the PDMS surface with the attached DNA in 1 μg/ml streptavidin in PBS buffer containing 0.4% BSA for 1 h, the surface was rinsed with PBST and PBS. Then, 4 μg/ml biotinylated antibodies were incubated for 1 h, followed by washing with PBST and PBS.

Contact Process and Fluorescence Readout. For the contact process a simple mechanical device was used to ensure that the two surfaces were aligned correctly and were parallel to each other. A force of ≈1.4 N was exerted to the 1-cm^2 PDMS surface for 10 min before the two surfaces were separated carefully, rinsed with double-distilled water, and dried with N_2. The bottom surface was then transferred to a GenePix 4000B microarray fluorescence scanner (Axon Instruments, Foster City, CA). Mean fluorescence transfer as well as background fluorescence intensities were determined by using NIH IMAGE software (National Institutes of Health, Bethesda; available at http://rsb.info.nih.gov/nih-image).

Results and Discussion

Fig. 1 schematically highlights the implementation of this format, which is similar to a microcontact printing setup (26–28), with the particular goal of discriminating specific from nonspecific interaction on a protein biochip. A short DNA duplex in unzip geometry served as a force sensor. One DNA strand was connected to a microstructured silicone elastomer surface (top surface) via a PEG spacer. The other DNA strand, which also carried the Cy3 fluorescence label, was attached to the ligand of the test complex, here a digoxigenin molecule. This particular type of force sensor was chosen for several reasons. It is known to provide a sequence-dependent force standard; 14 pN in this

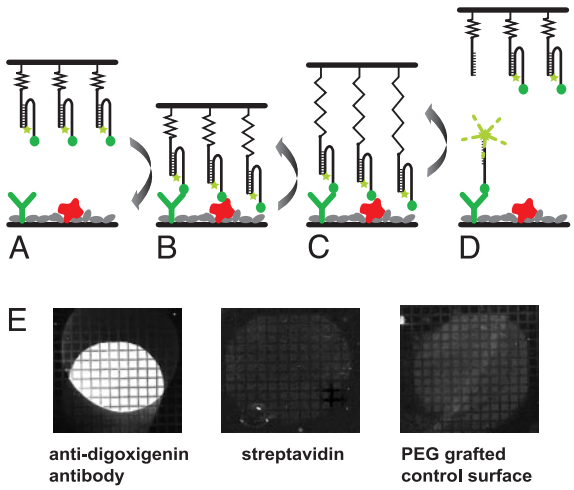

Fig. 1. Experimental realization of the differential force test. (*A*) DNA duplexes are connected to a microstructured silicone elastomer surface (top surface) via PEG spacers. The spacers are covalently bound to the silicone and in the next step are covalently attached to the 5′ end of one of the DNA strands. The complementary DNA strand contains a fluorescence label at the 5′ end and a 3′-digoxigenin label attached at the end of a poly(A) spacer sequence. (*B*) The PDMS surface is brought into contact with a second chip surface (bottom surface) containing spots of immobilized anti-digoxigenin antibodies, streptavidin proteins, or just the PEG passivation layer. (*C*) On separation of the two chip surfaces, the PEG spacers are extended and a force is built up in the molecular chains between the two surfaces. (*D*) As the two surfaces are further separated, the weakest molecular bond in each chain breaks, and the fluorescence label remains connected to the stronger bond. (*E*) After separation of the two surfaces, a fluorescence image of the bottom surface reveals strong fluorescence intensity on the spot carrying the anti-digoxigenin antibodies (*Left*), no fluorescence on the streptavidin spot (*Center*), and very little fluorescence on the PEG-coated control area (*Right*). The dark grids in the fluorescence images represent grooves of the microstructured PDMS. Note that in *Left* image the spots from the top and the bottom surface do not overlap entirely. Areas where the two spots do not overlap can be used as additional controls.

case (3, 29, 30). Because unzipping occurs in thermodynamic equilibrium, as long as the pulling velocity is kept below 200 nm/s, the unzipping force is independent of the separation rate and also independent of the duplex length (3, 30). The length may therefore be chosen according to the assay requirements such that the spontaneous off-rate is sufficiently slow to provide thermal stability (31). Note that the force threshold can easily be adapted by changing the base composition or the geometry of the DNA force sensor. To get to defined threshold forces above 65 pN, which corresponds to the shearing of long DNA duplexes (32, 33), nucleic acid derivatives like PNA or molecules such as streptavidin and biotin can be used as force sensors.

In Fig. 1*B*, the digoxigenin-baring silicone surface was allowed to adhere to a piece of a protein biochip with one spot of covalently attached polyclonal anti-digoxigenin IgG, one spot of streptavidin, and an untreated area. To displace the liquid between the two surfaces and obtain a homogeneous contact, a pressure of 14 kPa was exerted on the silicone surface. If one assumes a grafting density of 10^{12} PEG molecules per square centimeter, 14 kPa corresponds to a force of 1.4 pN per PEG, still well within the range of entropic forces (34). It should be noted that the adhesion of the polymer-coated silicone, and thus the interaction of the molecules at the interface between the two surfaces, is governed by local forces rather than the external force. Therefore, local surface roughness and distortions are compensated to a large degree by the softness of the polymer-coated silicone. Although the mobility of the binding partners is reduced by their polymeric attachment to the surfaces, the

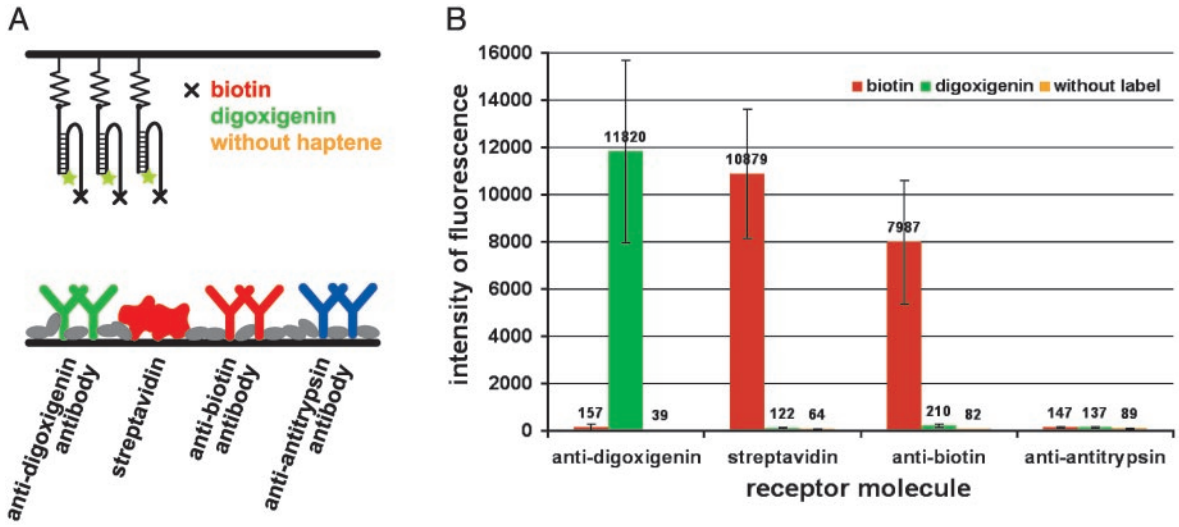

Fig. 2. Detection of specific haptene–protein interactions. (*A*) The transfer of two oligonucleotides coupled with different haptenes (biotin or digoxigenin) and one oligonucleotide without haptene label (top surface) onto spots containing the respective binding partners, as well as proteins not specific for the haptene (bottom surface), is determined. (*B*) Diagram showing the fluorescence intensities measured on (left to right) anti-digoxigenin, streptavidin, anti-biotin, and anti-antitrypsin spots on the bottom surface. Red bars correspond to biotin on the top surface, green bars correspond to digoxigenin, and yellow bars correspond to DNA without haptene. The ratio of specific to nonspecific transfer is always better than 50:1 for the two haptenes and their respective negative controls (transfer onto a specific binding partner versus transfer of the same haptene onto another ''nonspecific'' molecule).

reaction times are still faster than in corresponding conventional assays, because the local concentration of the binding partners in the gap between the two surfaces is extremely high. After 10 min in contact, the surfaces were separated (Fig. 1*C*), thereby stretching the polymeric anchors and gradually building up the force acting on the bonds and eventually rupturing the molecular interactions under investigation (Fig. 1*D*). The macroscopic force needed to pull the two surfaces apart is neither recorded nor analyzed. The interaction force is measured intrinsically and independently for each molecular bond. The asymmetry of the binding forces results in an asymmetry of the transfer of the reporter molecules, which is quantified, for example, by fluorescence imaging. Fig. 1*E* shows the anti-digoxigenin spot brightly illuminated by the Cy3 fluorescence. No fluorescence can be detected on the streptavidin spot, and only a faint pattern is recognizable on the untreated area. The dark grid stems from a trench pattern at the surface of the silicone, which allows for drainage of the liquid during contact formation and separation of the surfaces.

This sequence not only demonstrates the basic principle of the assay, but it furthermore helps to identify suitable reference force levels for the discrimination of specific and nonspecific interactions. This will play an important role in the following experiments. Obviously, the 14 pN, which we chose as reference force, are lower than this particular specific ligand–antibody binding force, resulting in efficient transfer of reporter molecules. At the same time this threshold is also high enough to overcome nonspecific interaction with the protein-coated surface of the streptavidin spot. The slight amount of transfer onto the untreated surface indicates a weak but measurable interaction, which, if needed, may be overcome by raising the threshold force. It might, however, also be caused by a few, but strongly interacting, molecules adhering to localized adhesion sites. In this case, improved blocking strategies might overcome this problem, as can be seen on the streptavidin spot.

Fig. 2 shows that the force threshold defined by the unzipping duplex is appropriate for a number of systems. Several small, haptene-like ligands were tested for their interaction with different proteins. The quantitative analysis (Fig. 2*B*) demonstrates the high discrimination ratio and the low level of nonspecific transfer. The fact that more fluorescence is observed on the streptavidin spot than on the anti-biotin spot most likely reflects a difference in the number of accessible binding sites after immobilization, because streptavidin contains more binding sites for biotin than the anti-biotin antibody. Furthermore, the anti-biotin antibodies were polyclonal antibodies, and the batch used may have also contained antibodies, which are not specific for biotin. The anti-digoxigenin antibodies are also polyclonal antibodies. However, a quantitative comparison of biotin transfer levels to those of digoxigenin is not possible, because thermodynamic data are not available. Nevertheless, according to supplier specification the affinity-purified anti-biotin antibodies showed an activity level well below 100%, whereas the affinity-purified anti-digoxigenin antibodies showed 100% activity, which is consistent with the higher transfer onto the anti-digoxigenin spot.

Having demonstrated the functionality of this assay, protein–protein interactions were then investigated. A set of four different antibodies was coupled to the DNA force sensors (Fig. 3*A*). The setup was assembled sequentially by covalently attaching receptor oligonucleotides to the PEG-coated silicone surface, then hybridizing the biotinylated unzip oligos and treating the surface with streptavidin. Finally, the biotinylated antibodies were attached to this pretreated surface (see *Methods*). The four protein antigens were immobilized on the adjacent chip surface by covalent attachment. Each antibody was tested against all antigens. The fluorescent readings of the corresponding spots are plotted in Fig. 3*B*. At the chosen reference force of 14 pN, we generally found $<13\%$ of nonspecific interaction with other proteins. The anti-rabbit antibody, which was the only polyclonal antibody in this set of experiments, showed rather high nonspecific interactions with GFP and human serum albumin (HSA). Because polyclonal antibodies are obtained from immunized animals (in this case goat), they also may contain fractions of antibodies that are not specific for the target protein or fractions that are specific for other proteins, like GFP or HSA. This may then lead to nonspecific signals. Note, however, that in this case the level of specific transfer onto rabbit antibodies was also significantly higher than the specific signals of the other anti-

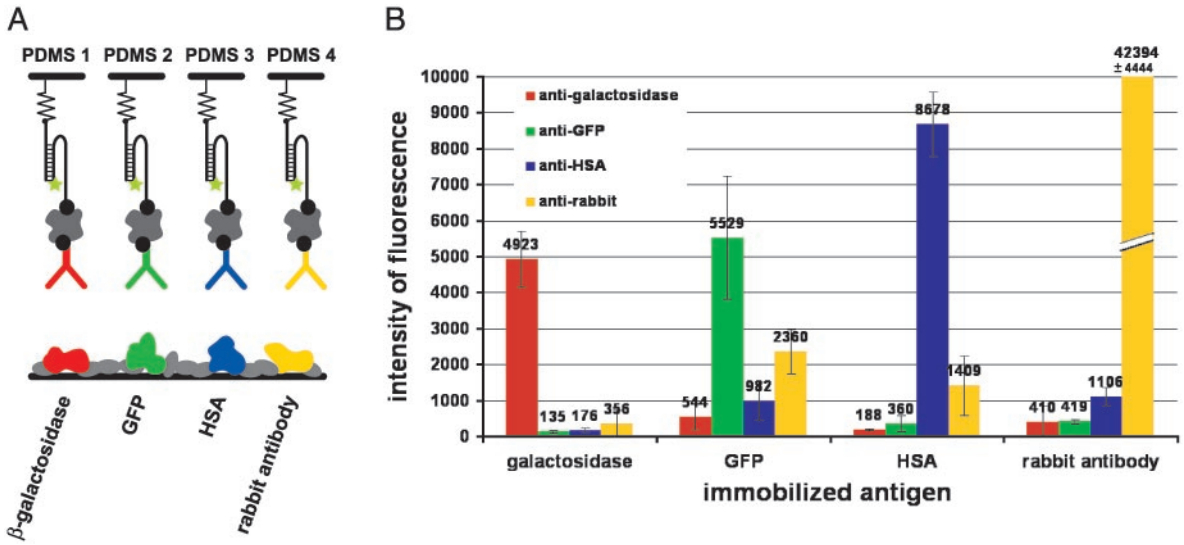

Fig. 3. Detection of specific antibody–antigen interactions. (*A*) The antibodies were coupled to the DNA force sensor (top surface) via biotin and streptavidin. Their corresponding antigens were immobilized on the bottom surface. Each antibody was tested against all antigens in the respective series (PDMS 1, monoclonal anti-β-galactosidase; PDMS 2, monoclonal anti-GFP; PDMS 3, monoclonal anti-HSA; PDMS 4, polyclonal anti-rabbit). (*B*) Fluorescence intensities measured on the bottom surface on spots containing (left to right) immobilized β-galactosidase, GFP, HSA, and rabbit antibodies. Red bars correspond to anti-β-galactosidase antibodies on the top surface, green bars correspond to anti-GFP, blue bars correspond to anti-HSA, and yellow bars correspond to anti-rabbit antibodies. The ratio of specific to nonspecific transfer is always better than 7:1 for the four antibodies and their respective negative controls (transfer onto a specific binding partner versus transfer of the same antibody onto another ''nonspecific'' molecule).

bodies, resulting in <6% background signal for the anti-rabbit antibody.

In the next step, we investigated the applicability of this differential force test to sandwich immunoassays (Fig. 4). Two different capture antibodies against a recombinant HCV antigen, as well as a mixture thereof, were covalently anchored at different spots on one chip surface (bottom surface). The HCV antigen was allowed to bind from solution, and the amount of bound antigen was then quantified by measuring the transfer of two different anti-HCV detection antibodies, as well as the mixture of both, from the second chip surface (top surface; assembly as in Fig. 3). The results are shown in Fig. 4*B*. The highest fluorescence intensities are observed on the spots with the high-affinity capture antibody (C2). The lowest fluorescence intensities are observed on spots with the capture antibody with lower affinity (C1), whereas the spots with mixed capture antibodies lie between the two. Furthermore, the fluorescence intensities are always higher for the high-affinity detection antibodies (D1) than for the low-affinity detection antibodies (D2). However, here the maximum is observed for the mixed system. This scenario is plausible, if one considers that the two detection antibodies bind to two different epitopes of the antigen, and therefore up to two antibodies can be transferred to one bound antigen. A quantitative analysis of sample con-

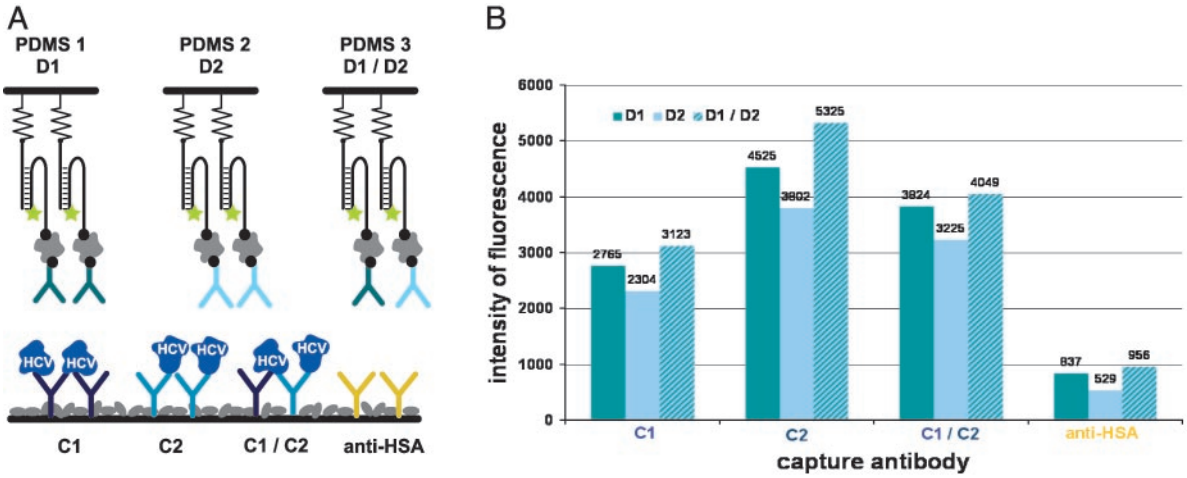

Fig. 4. An antibody sandwich assay for the detection of a hepatitis C virus antigen, based on the differential force test. (*A*) The detection antibodies are connected to the top surface via a DNA force sensor and a PEG spacer (PDMS 1, D1; PDMS 2, D2; PDMS 3, mixture of D1 and D2). Specific capture antibodies (C1, C2, and C1/C2), as well as one antibody binding human serum albumin as a negative control, are immobilized on the bottom surface. The antigen is bound by shaking the bottom surface in an antigen-containing solution. (*B*) Fluorescence intensities on the bottom surface on spots with (left to right) C1 capture antibodies, C2 capture antibodies, a mixture of C1 and C2 antibodies, and the negative control. Green bars represent D1 detection antibodies on the top chip surface, blue bars represent D2 detection antibodies, and striped bars represent a mixture of both. Specific to nonspecific ratios vary between 2.4:1 and 10.1:1 depending on the particular combination of sandwich antibodies, which were compared with the negative control.

centrations was also possible with this set-up, and the detection limit was comparable to a conventional sandwich setup, using the same type of capture surface and applying the detection antibodies from solution (data not shown).

In a more general context, this assay may be seen as a technology where a molecular species is brought to a certain position and delivered only if the interaction force at this position exceeds a chosen threshold, i.e., to probe whether a specific binding partner is present at a particular position. Here, we have only begun to exploit the potential of this new assay format. On the silicone surface (top), binding partners may be patterned in register to the pattern of molecules on the capture array (bottom); therefore, we have the option to probe each antigen bound to a capture array with a second antigen-specific binding partner. The second chip surface therefore allows for a second dimension of specific encoding. This is in sharp contrast to existing multiplexing formats, which rely either on only one antigen-specific molecular interaction or apply the second binding partners in an arbitrary manner by incubation from buffer solution (35–37). As a consequence, in conventional assays, the nonspecific and false-positive signals grow geometrically with the number of different molecular species probed in parallel (38) and thus limit the multiplexing level that can be achieved (39–43). In our case, nonspecific and false-positive signals are independent of array size. This allows for a large number of molecular interactions to be assessed in parallel by reducing the complexity of a multimarker assay to the simplicity of a single-marker ELISA.

We thank Edith Potthoff, Boris Steipe, Andreas Lankenau, and Claus Duschl for helpful discussions. Part of the project was supported by the Deutsche Forschungsgemeinschaft and the Bundesministerium für Bildung und Forschung.

1. Moy, V. T., Florin, E. L. & Gaub, H. G. (1994) *Science* **266,** 257–259.
2. Merkel, R., Nassoy, P., Leung, A., Ritchie, K. & Evans, E. (1999) *Nature* **397,** 50–53.
3. Rief, M., Clausen-Schaumann, H. & Gaub, H. E. (1999) *Nat. Struct. Biol.* **6,** 346–349.
4. Clausen-Schaumann, H., Seitz, M., Krautbauer, R. & Gaub, H. E. (2000) *Curr. Opin. Chem. Biol.* **4,** 524–530.
5. Williams, M. C. & Rouzina, I. (2002) *Curr. Opin. Struct. Biol.* **12,** 330–336.
6. Grandbois, M., Beyer, M., Rief, M., Clausen-Schaumann, H. & Gaub, H. E. (1999) *Science* **283,** 1727–1730.
7. Evans, E. (2001) *Annu. Rev. Biophys. Biomol. Struct.* **30,** 105–128.
8. Janshoff, A., Neitzert, M., Oberdorfer, Y. & Fuchs, H. (2000) *Angew. Chem. Int. Ed. Engl.* **39,** 3212–3237.
9. Hugel, T. & Seitz, M. (2001) *Macromol. Rapid Commun.* **22,** 989–1016.
10. Mehta, A. D., Rief, M., Spudich, J. A., Smith, D. A. & Simmons, R. M. (1999) *Science* **283,** 1689–1694.
11. Merkel, R. (2001) *Phys. Rep.* **346,** 343–385.
12. Binnig, G., Quate, C. F. & Gerber, C. (1986) *Phys. Rev. Lett.* **56,** 930–933.
13. Fritz, J., Baller, M. K., Lang, H. P., Rothuizen, H., Vettiger, P., Meyer, E., Guntherodt, H., Gerber, C. & Gimzewski, J. K. (2000) *Science* **288,** 316–318.
14. Arntz, Y., Seelig, J. D., Lang, H. P., Zhang, J., Hunziker, P., Ramseyer, J. P., Meyer, E., Hegner, M. & Gerber, C. (2003) *Nanotechnology* **14,** 86–90.
15. Minne, S. C., Yaralioglu, G., Manalis, S. R., Adams, J. D., Zesch, J., Atalar, A. & Quate, C. F. (1998) *Appl. Phys. Lett.* **72,** 2340–2342.
16. Albrecht, C., Blank, K., Lalic-Mülthaler, M., Hirler, S., Mai, T., Gilbert, I., Schiffmann, S., Bayer, T., Clausen-Schaumann, H. & Gaub, H. E. (2003) *Science* **301,** 367–370.
17. Florin, E.-L., Moy, V. T. & Gaub, H. E. (1994) *Science* **264,** 415–417.
18. Bustamante, C., Macosko, J. C. & Wuite, G. J. (2000) *Nat. Rev. Mol. Cell Biol.* **1,** 130–136.
19. Lavery, R., Lebrun, A., Allemand, J.-F., Bensimon, D. & Croquette, V. (2002) *J. Phys. Condens. Matter* **14,** R383–R414.
20. Viani, M. B., Schäffer, T. E., Chand, A., Rief, M., Gaub, H. E. & Hansma, P. K. (1999) *J. Appl. Phys.* **86,** 2258–2262.
21. Evans, E. & Ritchie, K. (1997) *Biophys. J.* **72,** 1541–1555.
22. Evans, E. (1999) *Biophys. Chem.* **82,** 83–97.
23. Schwesinger, F., Ros, R., Strunz, T., Anselmetti, D., Guntherodt, H. J., Honegger, A., Jermutus, L., Tiefenauer, L. & Pluckthun, A. (2000) *Proc. Natl. Acad. Sci. USA* **97,** 9972–9977.
24. Piehler, J., Brecht, A., Valiokas, R., Liedberg, B. & Gauglitz, G. (2000) *Biosens. Bioelectron.* **15,** 473–481.
25. Wilbur, J. L., Kumar, A., Kim, E. & Whitesides, G. M. (1994) *Adv. Mater.* **6,** 600–604.
26. Bernard, A., Renault, J. P., Michel, B., Bosshard, H. R. & Delamarche, E. (2000) *Adv. Mater.* **12,** 1067–1070.
27. Bernard, A., Fitzli, D., Sonderegger, P., Delamarche, E., Michel, B., Bosshard, H. R. & Biebuyck, H. (2001) *Nat. Biotechnol.* **19,** 866–869.
28. Xia, Y. & Whitesides, G. M. (1998) *Annu. Rev. Mater. Sci.* **28,** 153–184.
29. Essevaz-Roulet, B., Bockelmann, U. & Heslot, F. (1997) *Proc. Natl. Acad. Sci. USA* **94,** 11935–11940.
30. Bockelmann, U., Essevaz-Roulet, B. & Heslot, F. (1997) *Phys. Rev. Lett.* **79,** 4489–4492.
31. Strunz, T., Oroszlan, K., Schäfer, R. & Güntherodt, H.-J. (1999) *Proc. Natl. Acad. Sci. USA* **96,** 11277–11282.
32. Clausen-Schaumann, H., Rief, M., Tolksdorf, C. & Gaub, H. E. (2000) *Biophys. J.* **78,** 1997–2007.
33. Williams, M. C., Wenner, J. R., Rouzina, I. & Bloomfield, V. A. (2001) *Biophys. J.* **80,** 1932–1939.
34. Oesterhelt, F., Rief, M. & Gaub, H. E. (1999) *New J. Phys.* **1,** 6.1–6.11.
35. Ekins, R. P. (1989) *J. Pharm. Biomed. Anal.* **7,** 155–168.
36. Ekins, R. P. & Chu, F. (1994) *Trends Biotechnol.* **12,** 89–94.
37. Wagner, P. & Kim, R. (2002) *Curr. Drug Discov.* **5,** 23–28.
38. Abbott, A. (2002) *Nature* **415,** 112–114.
39. Mendoza, L. G., McQuary, P., Mongan, A., Gangadharan, R., Brignac, S. & Eggers, M. (1999) *BioTechniques* **27,** 778–788.
40. Huang, R. P. (2001) *J. Immunol. Methods* **255,** 1–13.
41. Mitchell, P. (2002) *Nat. Biotechnol.* **20,** 225–229.
42. MacBeath, G. (2002) *Nat. Genet.* **32,** Suppl. 2, 526–532.
43. Petach, H. & Glod, L. (2002) *Curr. Opin. Biotechnol.* **13,** 309–314.